The 9th European Congress on Computational Methods in Applied Sciences and Engineering
ECCOMAS Congress 2024
3–7 June 2024, Lisboa, Portugal

SIMULTANEOUS, DYNAMIC ANALYSIS OF STRUCTURAL ROPES AND MEMBRANES ON ALL LEVEL SETS

T.P. Fries[1,2] and M.W. Kaiser[3]

[1] Institute of Structural Analysis
Graz University of Technology
Lessingstr. 25, 8010 Graz, Austria
www.ifb.tugraz.at

[2]e-mail: fries@tugraz.at

[3]e-mail: michael.kaiser@tugraz.at

Key words: Finite strain theory, ropes and membranes, fictitious domain method, embedded domain method, Trace FEM, level-set method, structural dynamics

Summary. The level sets of scalar functions may imply the geometries of individual ropes and membranes. *All* level sets within an interval, considered in some bulk domain, define infinitely many geometries *at once*. A mechanical model is proposed which enables the simultaneous, *dynamic* analysis of all such geometries. For the solution of the governing equations, a tailored numerical method coined Bulk Trace FEM is employed for the spatial discretization, using higher-order background meshes in the bulk domains. The HHT-α method is used for the temporal discretization. Numerical results are presented that demonstrate the potential of the proposed mechanical model and numerical method.

1 Introduction

Ropes and membranes are curved, lower-dimensional, tensile structures embedded in a higher-dimensional space. The mechanical modeling of such structures in finite strain or large displacement theory as well as the numerical analysis based on the finite element method (FEM) are well-established [3, 2, 12]. The geometry of a lower-dimensional structure may be defined *explicitly* through a parametrization or *implicitly* by some (bounded) level set of a scalar function [18]. Previous works of the authors focus on reformulating and generalizing classical models for explicit geometries to the implicit case, see [12] for ropes and membranes, and [20, 22, 24] for shells. The authors extend their models from the analysis of *single* geometries to the simultaneous analysis of *all* geometries as implied by all level sets within some bulk domain, see [11, 10, 15] for membranes and [16] for shells. Herein, the situation is further extended from the static to the *dynamic* case by considering the inertia terms.

In Section 2, the mechanical model is formulated in terms of an initial boundary value problem (IBVP) in the bulk domain following [11, 10, 15]. Therefore, differential surface operators have to be defined in the bulk domain which refer to the curved level sets. Then, mechanical quantities may be defined and the governing equations in strong form are given. The spatial and temporal discretization of the IBVP in weak form is obtained in Section 3, serving as the basis for the

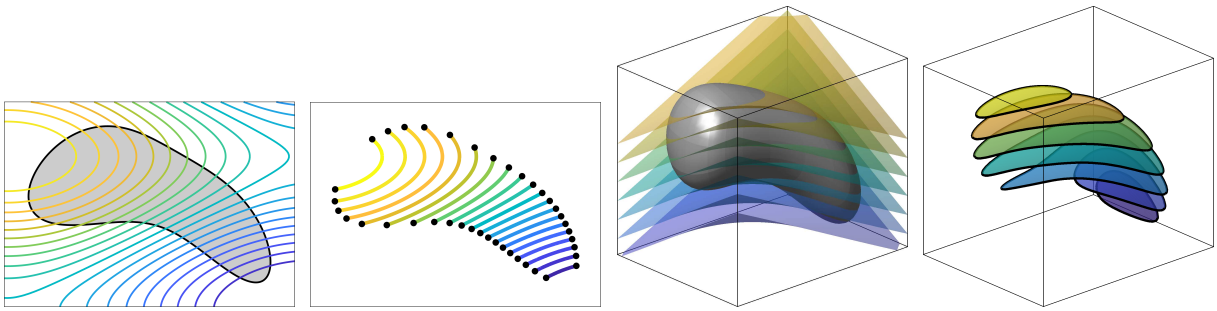

(a) Ω and level sets of ϕ (b) level sets Γ^c (c) Ω and level sets of ϕ (d) level sets Γ^c

Figure 1: Some bulk domain Ω and level-set function ϕ in two and three dimensions and the implied level sets Γ^c.

numerical treatment based on the Bulk Trace FEM [11] in space and the popular HHT-α method in time [14]. Therefore, the bulk domain is discretized by (higher-order) d-dimensional finite elements which do not conform to the level sets yet to the boundary of the bulk domain. The name of the method refers to the already established Trace FEM [17, 19, 13, 21, 22, 12] which is an embedded or fictitious domain method for the solution of BVPs on curved, implicitly defined manifolds, also using a d-dimensional background mesh for the analysis. However, the Bulk Trace FEM does *not* come with the usual issues of embedded domain methods in terms of (i) numerical integration, (ii) stabilization and (iii) enforcement of boundary conditions. Numerical results are presented in Section 4 using higher-order elements in the bulk domain. The paper ends in Section 5 with a summary and conclusions.

2 Mechanical model

In this section, the mechanical models for *dynamic* structural ropes and membranes considered simultaneously on all level sets over some bulk domain are defined, resulting in an initial boundary value problem (IBVP). The outline very closely follows [11, 10] for the *static* situation, with extensions to the dynamic case herein.

2.1 Undeformed and deformed configurations

As usual in finite strain or large displacement theory, an undeformed material configuration and a deformed spatial configuration are distinguished. With *configuration*, we refer to *all* level sets of a level-set function ϕ over some d-dimensional bulk domain, see Fig. 1. Let the undeformed bulk domain be $\Omega_{\boldsymbol{X}}$ and the level-set function $\phi\left(\boldsymbol{X}\right) : \Omega_{\boldsymbol{X}} \to \mathbb{R}$. Then, the individual undeformed domains of interest $\Gamma^c_{\boldsymbol{X}}$—being the set of membranes or ropes simultaneously considered—are each related to constant level-set values,

$$\Gamma^c_{\boldsymbol{X}} = \left\{\boldsymbol{X} \in \Omega_{\boldsymbol{X}} : \, \phi(\boldsymbol{X}) = c\right\}, \, c \in \left(\phi^{\min}, \, \phi^{\max}\right), \tag{1}$$

where $\phi^{\min}$ and $\phi^{\max}$ are either the infimum/supremum of the level-set function inside $\Omega_{\boldsymbol{X}}$ or user-defined values to restrict some bulk domain to a sub-interval of interest. The task is now to find the time-dependent displacement field of all structures implied by the individual level

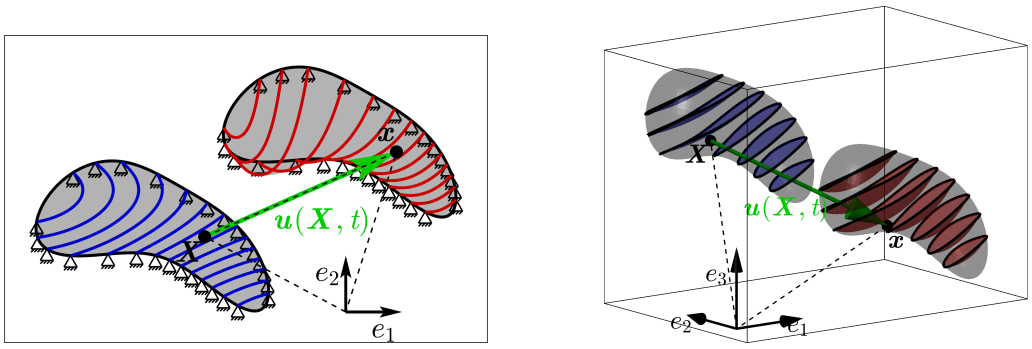

(a) situation in 2D (b) situation in 3D

Figure 2: Undeformed *material* configuration and deformed *spatial* configuration in two and three dimensions. The bulk domains $\Omega_{\boldsymbol{X}}$ and $\Omega_{\boldsymbol{x},t}$ are shown in gray. The undeformed level sets $\Gamma^c_{\boldsymbol{X}}$ are blue and the deformed level sets $\Gamma^c_{\boldsymbol{x},t}$ are red.

sets at once, see Fig. 2. That is, the deformed bulk domain

$$\Omega_{\boldsymbol{x},t} = \{\boldsymbol{x}\left(\boldsymbol{X},t\right) = \boldsymbol{X} + \boldsymbol{u}\left(\boldsymbol{X},t\right), \boldsymbol{X} \in \Omega_{\boldsymbol{X}}, t \in (0, t_{\text{end}})\}$$

is sought such that

$$\Gamma^c_{\boldsymbol{x},t} = \{\boldsymbol{x} \in \Omega_{\boldsymbol{x},t} : \phi(\boldsymbol{x}) = c\}, c \in \left(\phi^{\min}, \phi^{\max}\right), t \in (0, t_{\text{end}})$$

are the deformed structures. Illustratively, plotting selected level sets of $\phi\left(\boldsymbol{X}\right)$ in $\Omega_{\boldsymbol{X}}$ shows some undeformed structures whereas plotting the same level sets of $\phi\left(\boldsymbol{x}\right)$ in $\Omega_{\boldsymbol{x},t}$ represents the resulting deformed structures as shown in Fig. 2. In order to define the corresponding IBVP, we need to (i) define (co-)normal vector fields, (ii) differential operators, and (iii) mechanical vector and tensor fields. Further details are given in [11, 15].

2.2 Normal and conormal vectors

The boundary of the undeformed bulk domain $\partial\Omega_{\boldsymbol{X}}$ features a unit normal vector (field) $\boldsymbol{M}(\boldsymbol{X})$, $\boldsymbol{X} \in \partial\Omega_{\boldsymbol{X}}$. Instead, the unit normal vector (field) $\boldsymbol{N}(\boldsymbol{X})$ on the level sets $\Gamma^c_{\boldsymbol{X}}$ in the whole bulk domain $\Omega_{\boldsymbol{X}}$ is obtained from the gradient of the level-set function,

$$\boldsymbol{N}(\boldsymbol{X}) = \frac{\boldsymbol{N}^\star}{\|\boldsymbol{N}^\star\|} \quad \text{with} \quad \boldsymbol{N}^\star = \nabla_{\boldsymbol{X}}\phi\left(\boldsymbol{X}\right), \ \boldsymbol{X} \in \Omega_{\boldsymbol{X}}. \tag{2}$$

One may then also construct the projector field $\mathbf{P}\left(\boldsymbol{X}\right) \in \mathbb{R}^{d\times d}$, $\boldsymbol{X} \in \Omega_{\boldsymbol{X}}$ as $\mathbf{P}(\boldsymbol{X}) = \mathbf{I} - \boldsymbol{N} \otimes \boldsymbol{N}$. The unit *conormal* vectors $\boldsymbol{Q}(\boldsymbol{X})$ on $\partial\Omega_{\boldsymbol{X}}$ are in the tangent plane of the corresponding level sets at $\partial\Gamma^c_{\boldsymbol{X}}$ and yet normal to $\boldsymbol{N}(\boldsymbol{X})$ from above. In case of two-dimensional bulk domains, $d = 2$, see Fig. 3(a), these vectors immediately result from the normal vectors $\boldsymbol{N}$. For three-dimensional bulk domains, $d = 3$, see Fig. 3(b), one needs to first generate tangent vector fields $\boldsymbol{T}(\boldsymbol{X})$ on $\partial\Omega_{\boldsymbol{X}}$ using cross products of the normal vector fields from above, $\boldsymbol{T} = \boldsymbol{M} \times \boldsymbol{N}$, and then $\boldsymbol{Q} = \frac{\boldsymbol{Q}^\star}{\|\boldsymbol{Q}^\star\|}$ with $\boldsymbol{Q}^\star = \boldsymbol{N} \times \boldsymbol{T}$. Similar vector fields may be obtained with respect to the *deformed* bulk domain $\Omega_{\boldsymbol{x},t}$, however, it is then noted that they are time-dependent, i.e., $\boldsymbol{n}(\boldsymbol{x}\left(\boldsymbol{X},t\right))$, $\boldsymbol{q}(\boldsymbol{x}\left(\boldsymbol{X},t\right))$ etc.

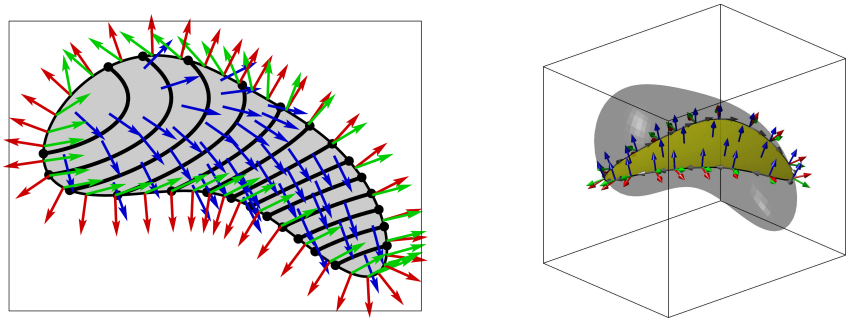

(a) vectors $\boldsymbol{N}$, $\boldsymbol{M}$, $\boldsymbol{Q}$ (b) vectors $\boldsymbol{N}$, $\boldsymbol{M}$, $\boldsymbol{Q}$, $\boldsymbol{T}$

Figure 3: Vector fields in the bulk domain $\Omega_{\boldsymbol{X}}$ and on the boundary $\partial\Omega_{\boldsymbol{X}}$ in (a) two and (b) three dimensions (for clarity, only one level set is shown in 3D). Normal vectors $\boldsymbol{N}$ with respect to the level sets $\Gamma^c_{\boldsymbol{X}}$ in $\Omega_{\boldsymbol{X}}$ are shown in blue. Normal vectors $\boldsymbol{M}$ with respect to $\partial\Omega_{\boldsymbol{X}}$ are red, tangential vectors $\boldsymbol{T}$ are gray and conormal vectors $\boldsymbol{Q}$ are green.

2.3 Differential operators

It is important to distinguish (classical) differential operators acting in the bulk space from those acting on the level sets which may be called *tangential* or *surface* operators. Here, these operators are defined with respect to the undeformed configuration but extend straightforwardly to the time-dependent, deformed situation as well. The *surface gradient* of a scalar function $f(\boldsymbol{X}) : \Omega_{\boldsymbol{X}} \to \mathbb{R}$ results as [5, 7, 23]

$$\nabla^{\Gamma}_{\boldsymbol{X}} f = \mathbf{P} \cdot \nabla_{\boldsymbol{X}} f, \tag{3}$$

where $\nabla_{\boldsymbol{X}} f$ is the classical gradient in the undeformed d-dimensional bulk domain. For the directional and covariant surface gradients of some *vector* function $\boldsymbol{u}(\boldsymbol{X}) : \Omega_{\boldsymbol{X}} \to \mathbb{R}^d$, one obtains

$$\nabla^{\Gamma,\mathrm{dir}}_{\boldsymbol{X}} \boldsymbol{u} = \nabla_{\boldsymbol{X}} \boldsymbol{u} \cdot \mathbf{P}, \qquad \nabla^{\Gamma,\mathrm{cov}}_{\boldsymbol{X}} \boldsymbol{u} = \mathbf{P} \cdot \nabla_{\boldsymbol{X}} \boldsymbol{u} \cdot \mathbf{P},$$

respectively. Concerning the *surface divergence* of vector functions $\boldsymbol{u}(\boldsymbol{X})$ and tensor functions $\mathbf{A}(\boldsymbol{X}) : \Omega_{\boldsymbol{X}} \to \mathbb{R}^{d\times d}$, there holds

$$\mathrm{Div}_{\Gamma}\, \boldsymbol{u}(\boldsymbol{X}) = \mathrm{tr}\left(\nabla^{\Gamma,\mathrm{dir}}_{\boldsymbol{X}} \boldsymbol{u}\right) = \mathrm{tr}\left(\nabla^{\Gamma,\mathrm{cov}}_{\boldsymbol{X}} \boldsymbol{u}\right) =: \nabla^{\Gamma}_{\boldsymbol{X}} \cdot \boldsymbol{u}, \tag{4}$$

$$\mathrm{Div}_{\Gamma}\, \mathbf{A}(\boldsymbol{X}) = \begin{bmatrix} \mathrm{Div}_{\Gamma}\,(A_{11}, A_{12}, A_{13}) \\ \mathrm{Div}_{\Gamma}\,(A_{21}, A_{22}, A_{23}) \\ \mathrm{Div}_{\Gamma}\,(A_{31}, A_{32}, A_{33}) \end{bmatrix} =: \nabla^{\Gamma}_{\boldsymbol{X}} \cdot \mathbf{A}. \tag{5}$$

2.4 Mechanical quantities

With the displacement field $\boldsymbol{u}(\boldsymbol{X}, t) : \mathbb{R}^d \to \mathbb{R}^d$, and $\boldsymbol{x}(\boldsymbol{X}, t) = \boldsymbol{X} + \boldsymbol{u}(\boldsymbol{X}, t)$, the resulting *bulk deformation gradient* is

$$\mathbf{F}_{\Omega} = \nabla_{\boldsymbol{X}} \boldsymbol{x}(\boldsymbol{X}, t) = \mathbf{I} + \nabla_{\boldsymbol{X}} \boldsymbol{u}(\boldsymbol{X}, t), \tag{6}$$

where $\mathbf{I}$ is the $(d \times d)$-identity matrix. Note that $\nabla_{\boldsymbol{X}}$ is the classical gradient with respect to the undeformed bulk domain $\Omega_{\boldsymbol{X}}$ and $\nabla_{\boldsymbol{x}}$ with respect to $\Omega_{\boldsymbol{x},t}$. Based on these definitions, the

surface deformation gradient $\mathbf{F}_\Gamma$ is

$$\mathbf{F}_\Gamma = \nabla_{\boldsymbol{X}}^{\Gamma,\mathrm{dir}} \boldsymbol{x}\left(\boldsymbol{X},t\right) = \mathbf{I} + \nabla_{\boldsymbol{X}}^{\Gamma,\mathrm{dir}} \boldsymbol{u}\left(\boldsymbol{X},t\right). \tag{7}$$

The directional and tangential Green-Lagrange strain tensors are then defined as

$$\mathbf{E}_{\mathrm{dir}} = {}^1\!/_2 \cdot \left(\mathbf{F}_\Gamma^{\mathrm{T}} \cdot \mathbf{F}_\Gamma - \mathbf{I}\right), \qquad \mathbf{E}_{\mathrm{tang}} = \mathbf{P} \cdot \mathbf{E}_{\mathrm{dir}} \cdot \mathbf{P}, \tag{8}$$

respectively. When considering a Saint Venant–Kirchhoff solid, the second Piola-Kirchhoff stress tensor results as

$$\mathbf{S} \;\; = \;\; \lambda \cdot \mathrm{trace}\left(\mathbf{E}_{\mathrm{tang}}\right) \cdot \mathbf{P} + 2\mu \mathbf{E}_{\mathrm{tang}}, \tag{9}$$

with $\mathbf{S}$ being tangential to $\Gamma_{\boldsymbol{X}}^{\mathrm{c}}$, λ and μ are the Lamé constants. For given Young's modulus E and Poisson's ratio ν, there holds $\lambda = \frac{E\cdot\nu}{1-\nu^2}$, $\mu = \frac{E}{2(1+\nu)}$ for membranes, and $\lambda = 0$, $\mu = \frac{E}{2}$ for ropes. The Cauchy stress tensor reads

$$\boldsymbol{\sigma} = \frac{1}{\Lambda} \cdot \mathbf{F}_\Gamma \cdot \mathbf{S} \cdot \mathbf{F}_\Gamma^{\mathrm{T}} \qquad \text{with} \qquad \Lambda = \frac{\|\nabla_{\boldsymbol{x}}\phi\|}{\|\nabla_{\boldsymbol{X}}\phi\|} \cdot \det \mathbf{F}_\Omega, \tag{10}$$

where Λ is a *line* stretch for ropes and an *area* stretch for membranes when undergoing the displacement. The first Piola-Kirchhoff stress tensor is given by $\mathbf{K} = \mathbf{F}_\Gamma \cdot \mathbf{S}$.

2.5 Governing equations

The equilibrium on all level sets $\Gamma_{\boldsymbol{x},t}^{\mathrm{c}}$ with respect to the deformed configuration $\Omega_{\boldsymbol{x},t}$ may be stated as

$$\varrho \cdot \{A,\tau\} \cdot \ddot{\boldsymbol{u}} - \mathrm{div}_\Gamma\, \boldsymbol{\sigma}(\boldsymbol{x}) = \boldsymbol{f}(\boldsymbol{x}) \quad \forall \boldsymbol{x} \in \Omega_{\boldsymbol{x},t},\ t \in (0, t_{\mathrm{end}}),$$

where, for ropes, A is the cross-section or, for membranes, τ is the thickness. The density in the deformed configuration is $\varrho = \varrho_0/\Lambda$, with $\varrho_0 \in \mathbb{R}^+$ being some constant density in the undeformed configuration. It is common to express this equilibrium purely based on quantities in the undeformed configuration as

$$\varrho_0 \cdot \{A,\tau\} \cdot \ddot{\boldsymbol{u}}\left(\boldsymbol{X},t\right) - \mathrm{Div}_\Gamma\, \mathbf{K}(\boldsymbol{X},t) = \boldsymbol{F}(\boldsymbol{X},t) \quad \forall \boldsymbol{X} \in \Omega_{\boldsymbol{X}},\ t \in (0, t_{\mathrm{end}}). \tag{11}$$

One may then identify the field equations of the IBVP modeling the mechanics of membranes (and ropes) simultaneously on *all* level sets in some bulk domain through Eq. (8) (kinematics), Eq. (9) (constitutive equation), and Eq. (11) (equilibrium). Suitable initial and boundary conditions for displacements and tractions complete the definition of the IBVP.

3 Weak form and numerical analysis

For the simultaneous analysis of structures implied by *all* level sets over a bulk domain as proposed herein, the bulk domain $\Omega_{\boldsymbol{X}}$ is (spatially) discretized by a background mesh which is conforming to the boundary $\partial\Omega_{\boldsymbol{X}}$ (and, hence, also $\partial\Gamma_{\boldsymbol{X}}^{\mathrm{c}}$), yet typically *not* conforming to the individual level sets $\Gamma_{\boldsymbol{X}}^{\mathrm{c}}$ of ϕ, see Fig. 4. This approach was previously labeled the Bulk Trace FEM in [11, 10, 15] and was also used in [8, 6, 1] for transport applications. For the time discretization, the popular HHT-α time-stepping method is employed [14].

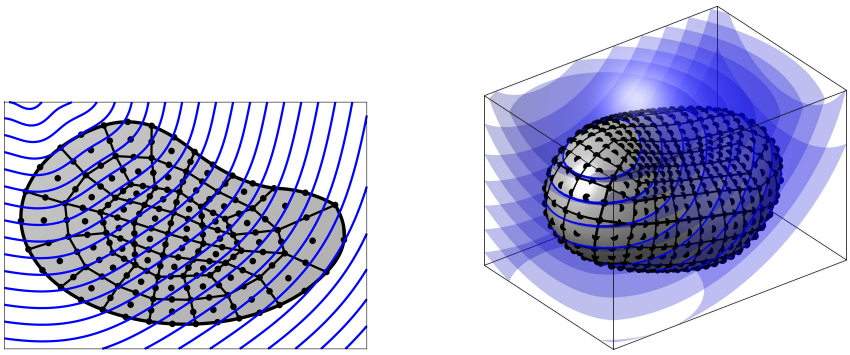

(a) $\Omega_{\boldsymbol{X}} \in \mathbb{R}^2$ (b) $\Omega_{\boldsymbol{X}} \in \mathbb{R}^3$

Figure 4: In the Bulk Trace FEM, the bulk domain is discretized by d-dimensional, possibly higher-order elements which do not conform to the level sets.

For the FEM-analysis in space, a discretized weak form is required. For brevity, the proper introduction of suitable test and trial functions is omitted here, however, it is noted that classical C_0-continuous finite elements are later employed in the numerical results. We first obtain the weak form of Eq. (11) on *one* selected level set $\Gamma_{\boldsymbol{X}}^c$ in the usual way by (1) multiplying with a test function, (2) integrating over the domain $\Gamma_{\boldsymbol{X}}^c$, and (3) applying the divergence theorem on manifolds [4, 5], resulting into

$$\int_{\Gamma_{\boldsymbol{X}}^c} \varrho_0 \cdot \{A, \tau\} \cdot \boldsymbol{w} \cdot \ddot{\boldsymbol{u}} \, \mathrm{d}\Gamma + \int_{\Gamma_{\boldsymbol{X}}^c} \nabla_{\boldsymbol{X}}^{\Gamma,\mathrm{dir}} \boldsymbol{w} : \mathbf{K} \, \mathrm{d}\Gamma = \int_{\Gamma_{\boldsymbol{X}}^c} \boldsymbol{w} \cdot \boldsymbol{F} \, \mathrm{d}\Gamma + \int_{\partial\Gamma_{\boldsymbol{X}}^c} \boldsymbol{w} \cdot \hat{\boldsymbol{H}} \, \mathrm{d}\partial\Gamma, \tag{12}$$

where $\hat{\boldsymbol{H}} = \mathbf{K} \cdot \boldsymbol{Q}$ are tractions. Note that in Eq. (12), the curvature term $\int_{\Gamma_{\boldsymbol{X}}^c} \varkappa \cdot \boldsymbol{w} \cdot (\mathbf{K} \cdot \boldsymbol{N}) \, \mathrm{d}\Gamma$ vanished due to $\mathbf{K} \cdot \boldsymbol{N} = 0$.

Next, we integrate over all level sets in the bulk domain and make use of the *co-area formula* [6, 9]

$$\int_{\phi^{\min}}^{\phi^{\max}} \int_{\Gamma_{\boldsymbol{X}}^c} f(\boldsymbol{X}) \; \mathrm{d}\Gamma \, \mathrm{d}c = \int_{\Omega_{\boldsymbol{X}}} f(\boldsymbol{X}) \cdot \|\nabla_{\boldsymbol{X}} \phi\| \; \mathrm{d}\Omega \tag{13}$$

and its counterpart for integrating over the boundary $\partial\Gamma_{\boldsymbol{X}}^c$,

$$\int_{\phi^{\min}}^{\phi^{\max}} \int_{\partial\Gamma_{\boldsymbol{X}}^c} f(\boldsymbol{X}) \cdot \boldsymbol{Q} \, \mathrm{d}\partial\Gamma \, \mathrm{d}c = \int_{\partial\Omega_{\boldsymbol{X}}} f(\boldsymbol{X}) \cdot \boldsymbol{Q} \cdot (\boldsymbol{Q} \cdot \boldsymbol{M}) \cdot \|\nabla_{\boldsymbol{X}} \phi\| \; \mathrm{d}\partial\Omega. \tag{14}$$

Note that on the right hand side, the conormal vectors $\boldsymbol{Q}$ with respect to $\Gamma_{\boldsymbol{X}}^c$ as well as the normal vectors $\boldsymbol{M}$ on $\partial\Omega_{\boldsymbol{X}}$ are involved.

When using Eq. (13) for the domain integrals in Eq. (12) and Eq. (14) for the boundary integrals, one obtains

$$\int_{\Omega_{\boldsymbol{X}}} \varrho_0 \cdot \{A, \tau\} \cdot \boldsymbol{w} \cdot \ddot{\boldsymbol{u}} \cdot \|\nabla_{\boldsymbol{X}} \phi\| \; \mathrm{d}\Omega + \int_{\Omega_{\boldsymbol{X}}} \nabla_{\boldsymbol{X}}^{\Gamma,\mathrm{dir}} \boldsymbol{w} : \mathbf{K}(\boldsymbol{u}) \cdot \|\nabla_{\boldsymbol{X}} \phi\| \; \mathrm{d}\Omega = \tag{15}$$

$$\int_{\Omega_{\boldsymbol{X}}} \boldsymbol{w} \cdot \boldsymbol{F} \cdot \|\nabla_{\boldsymbol{X}} \phi\| \; \mathrm{d}\Omega + \int_{\partial\Omega_{\boldsymbol{X},\mathrm{N}}} \boldsymbol{w} \cdot \hat{\boldsymbol{H}} \cdot (\boldsymbol{Q} \cdot \boldsymbol{M}) \cdot \|\nabla_{\boldsymbol{X}} \phi\| \; \mathrm{d}\partial\Omega. \tag{16}$$

It is noted that only first-order derivatives in space are involved, allowing for the use of classical C_0-continuous finite elements in the corresponding *discrete* weak form. For the time discretization of the remaining second-order initial value problem, the HHT-α method is used [14].

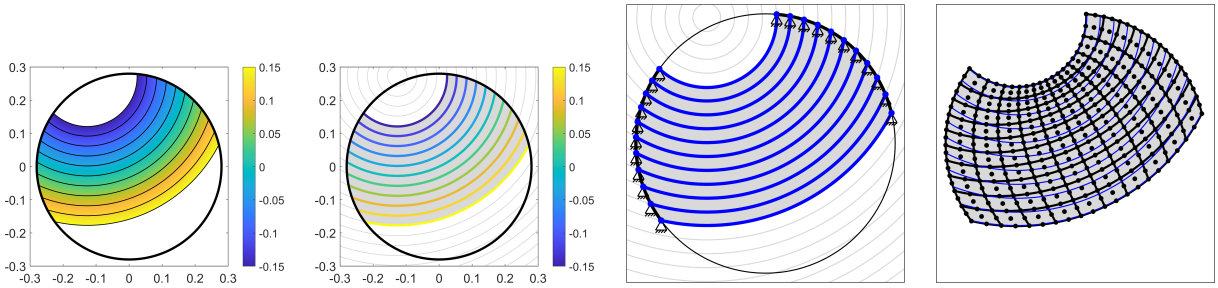

(a) $\Omega_{\boldsymbol{X}}$ and $\phi(\boldsymbol{X})$ (b) $\Omega_{\boldsymbol{X}}$ and $\phi(\boldsymbol{X})$ (c) mechanical setup (d) example mesh

Figure 5: Setup of test case: (a) and (b) show two alternative visualizations of the bulk domain in the level-set interval $(-0.15, 0.15)$, (c) shows the implied mechanical setup for some selected level sets, (d) shows an example mesh composed by quadratic Lagrange-elements.

4 Numerical results

A set of ropes is considered whose shapes are implied by the level set function $\phi(\boldsymbol{X}) = \|\boldsymbol{X} - \boldsymbol{X}_{\mathrm{C}}\| - R_{\mathrm{C}}$ with $\boldsymbol{X}_{\mathrm{C}} = \left[-0.3 \cdot \sin 25^{\circ}, 0.3 \cdot \cos 25^{\circ}\right]^{\mathrm{T}}$ and $R_{\mathrm{C}} = 0.3$. The level set interval between $\phi^{\min} = -0.15$ and $\phi^{\max} = +0.15$ is considered. The undeformed bulk domain $\Omega_{\boldsymbol{X}}$ is the part of a circle with radius $R_{\Omega} = 0.28$ around the origin where $\phi^{\min} \leq \phi \leq \phi^{\max}$, see Figs. 5(a) and (b) for two alternative visualizations. The implied mechanical setup is seen in Fig. 5(c) for some selected ropes (level sets). Pin supports are present at the end points of the ropes, that is, the thick black line in Fig. 5(c) is the Dirichlet boundary $\partial\Omega_{\boldsymbol{X},\mathrm{D}}$ where $\boldsymbol{u} = \boldsymbol{0}$ is prescribed. Test case parameters are defined as density $\varrho_0 = 400$, cross section $A = 1$, Young's modulus $E = 5\,000$, and body forces $\boldsymbol{F} = [0, -1\,000]$. The considered time interval is $t \in (0, 1)$.

For the numerical analyses, sequences of meshes with various orders and element numbers have been systematically employed. An example mesh composed of 10×10 quadratic Lagrange elements is shown in Fig. 5(d). Various time steps in the HHT-α method have been studied, the results presented here are obtained with 200 time steps, hence, $\Delta t = 0.005$. The time-dependent, deformed bulk domains $\Omega_{\boldsymbol{x},t}$ at various instances in time are seen in Fig. 6. Finally, the time-dependent, stored elastic energy, integrated over the bulk domain as

$$\mathfrak{e}(\boldsymbol{u}) = \frac{1}{2}\int_{\Omega_{\boldsymbol{x},t}} \mathbf{e}_{\mathrm{tang}}(\boldsymbol{u}) : \boldsymbol{\sigma}(\boldsymbol{u}) \cdot \|\nabla_{\boldsymbol{x}}\phi\| \, \mathrm{d}\Omega, \tag{17}$$

$$= \frac{1}{2}\int_{\Omega_{\boldsymbol{X}}} \mathbf{E}_{\mathrm{tang}}(\boldsymbol{u}) : \mathbf{S}(\boldsymbol{u}) \cdot \|\nabla_{\boldsymbol{X}}\phi\| \, \mathrm{d}\Omega, \tag{18}$$

is given in Fig. 7 for different meshes, confirming the expected convergence for increasing element numbers and orders.

5 Conclusions

Initial boundary value problems (IBVPs) are proposed for the simultaneous, dynamic analysis of structural ropes and membranes as implied by all level sets over some bulk domain. The resulting IBVPs are discretized using background meshes in the (undeformed) bulk domains and the Bulk Trace FEM, combined with the HHT-α method as the time-stepping scheme. The elements do not usually align with the geometries of the ropes and membranes which

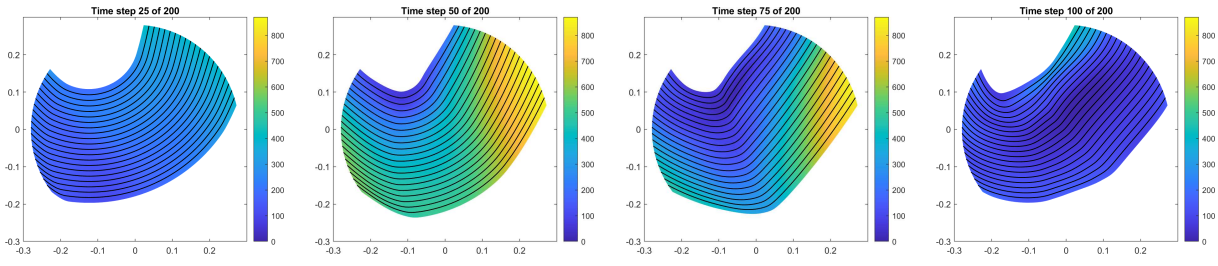

(a) $t = 0.125$ (b) $t = 0.25$ (c) $t = 0.375$ (d) $t = 0.5$

(e) $t = 0.625$ (f) $t = 0.75$ (g) $t = 0.875$ (h) $t = 1$

Figure 6: Results at different time steps: The figures show von Mises stresses in the time-dependent, deformed bulk domain $\Omega_{\boldsymbol{x},t}$ plus some selected level sets as black lines.

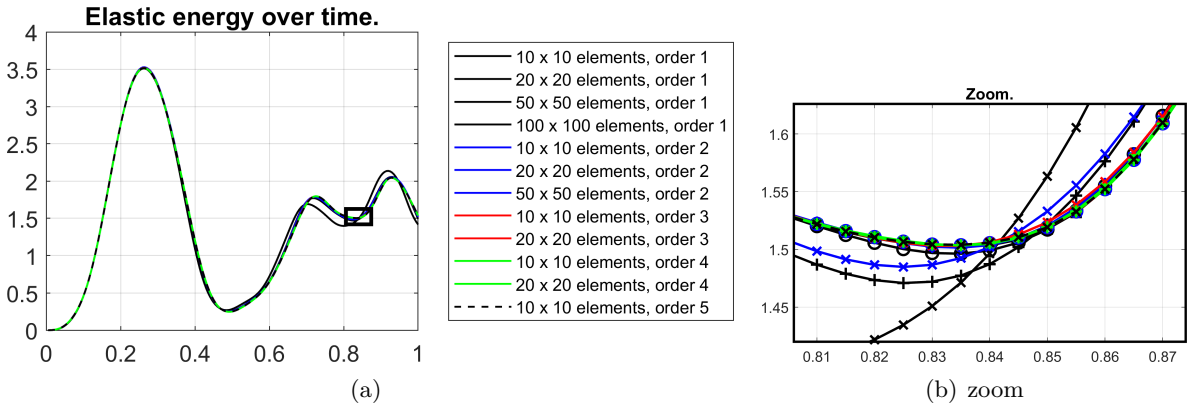

(a) (b) zoom

Figure 7: Stored elastic energy $\mathfrak{e}(\boldsymbol{u})$ in time with different orders and element numbers.

resembles the Trace FEM, however, *without* the usual challenges of fictitious domain methods in this context. Numerical results confirm the success of the proposed mechanical models and numerical framework. We envision large potential when combined with conventional (dynamic) bulk models for d-dimensional structures, introducing a new concept for advanced material models, possibly labeled continuously embedded sub-structure models with possible applications, e.g., in textile, biomechanical or fiber-reinforced structures and composite laminates.

REFERENCES

[1] Burger, M.: Finite element approximation of elliptic partial differential equations on implicit surfaces. *Comput. Vis. Sci.*, **12**, 87–100, 2009.

[2] Chapelle, D.; Bathe, K.J.: *The Finite Element Analysis of Shells – Fundamentals.* Computational Fluid and Solid Mechanics. Springer, Berlin, 2011.

[3] Ciarlet, P.G.: *Mathematical elasticity, III: Theory of shells.* Elsevier, Amsterdam, 1997.

[4] Delfour, M.C.; Zolésio, J.P.: Tangential Differential Equations for Dynamical Thin-Shallow Shells. *Journal of Differential Equations*, **128**, 125–167, 1996.

[5] Delfour, M.C.; Zolésio, J.P.: *Shapes and geometries—Metrics, Analysis, Differential Calculus, and Optimization.* SIAM, Philadelphia, PA, 2011.

[6] Dziuk, G.; Elliott, C.M.: Eulerian finite element method for parabolic PDEs on implicit surfaces. *Interfaces and Free Boundaries*, **10**, 2008.

[7] Dziuk, G.; Elliott, C.M.: An Eulerian approach to transport and diffusion on evolving implicit surfaces. *Computing and Visualization in Science*, **13**, 17–28, 2010.

[8] Dziuk, G.; Elliott, C.M.: Finite element methods for surface PDEs. *Acta Numerica*, **22**, 289–396, 2013.

[9] Federer, H.: *Geometric measure theory.* Springer, New York, 1969.

[10] Fries, T.P.; Kaiser, M.W.: The Bulk Trace FEM for the Simultaneous Solution of Structural Membranes on all Level-sets over a Bulk Domain. *Proceedings in Applied Mathematics and Mechanics*, Vol. 23, John Wiley & Sons, Chichester, 2023.

[11] Fries, T.P.; Kaiser, M.W.: On the Simultaneous Solution of Structural Membranes on all Level Sets within a Bulk Domain. *Comp. Methods Appl. Mech. Engrg.*, **415**, 116223, 2023.

[12] Fries, T.P.; Schöllhammer, D.: A unified finite strain theory for membranes and ropes. *Comp. Methods Appl. Mech. Engrg.*, **365**, 113031, 2020.

[13] Grande, J.; Lehrenfeld, C.; Reusken, A.: Analysis of a high-order trace finite element method for PDEs on level set surfaces. *SIAM J. Numer. Anal.*, **56**, 228–255, 2018.

[14] Hilber, H.M.; Hughes, T.J.R.; Taylor, R.L.: Improved Numerical Dissipation for Time Integration Algorithms in Structural Dynamics. *Earthquake Engineering and Structural Dynamics*, **5**, 283–292, 1977.

[15] Kaiser, M.W.; Fries, T.P.: Simultaneous solution of ropes and membranes on all level sets within a bulk domain. *Proceedings in Applied Mathematics and Mechanics*, Vol. 23, John Wiley & Sons, Chichester, 2023.

[16] Kaiser, M.W.; Fries, T.P.: Simultaneous analysis of continuously embedded Reissner-Mindlin shells in 3D bulk domains. *Internat. J. Numer. Methods Engrg.*, **e7495**, 0–0, 2024.

[17] Olshanskii, M.A.; Reusken, A.: Trace finite element methods for PDEs on surfaces. In *Geometrically Unfitted Finite Element Methods and Applications*. (Bordas, S.P.A.; Burman, E.; Larson, M.G.; Olshanskii, M.A.; Olshanskii, M.A., Eds.), Vol. 121, *Lecture notes in computational science and engineering*, Springer Nature, Cham, 211–258, 2017.

[18] Osher, S.; Fedkiw, R.P.: *Level Set Methods and Dynamic Implicit Surfaces*. Springer, Berlin, 2003.

[19] Reusken, A.: Analysis of trace finite element methods for surface partial differential equations. *IMA J Numer Anal*, **35**, 1568–1590, 2015.

[20] Schöllhammer, D.; Fries, T.P.: Kirchhoff-Love shell theory based on Tangential Differential Calculus. *Proceedings in Applied Mathematics and Mechanics*, Vol. 18, John Wiley & Sons, Chichester, 2018.

[21] Schöllhammer, D.; Fries, T.P.: Kirchhoff-Love shell theory based on tangential differential calculus. *Comput. Mech.*, **64**, 113–131, 2019.

[22] Schöllhammer, D.; Fries, T.P.: Reissner-Mindlin shell theory based on tangential differential calculus. *Comp. Methods Appl. Mech. Engrg.*, **352**, 172–188, 2019.

[23] Schöllhammer, D.; Fries, T.P.: A unified approach for shell analysis on explicitly and implicitly defined surfaces. In *Proceedings of the IASS Annual Symposium 2019 (Form and Force, Structural Membranes 2019)*. (Lázaro, C.; Bletzinger, K.U.; Oñate, E.; Oñate, E., Eds.), Barcelona, Spain, 750–757, 2019.

[24] Schöllhammer, D.; Fries, T.P.: A higher-order Trace finite element method for shells. *Internat. J. Numer. Methods Engrg.*, **122**, 1217–1238, 2021.